Available online at www.sciencedirect.com
ScienceDirect
Journal of Catalysis 251 (2007) 443–452
JOURNAL OF CATALYSIS
www.elsevier.com/locate/jcat

Effects of zeolite structure and composition on the synthesis of dimethyl carbonate by oxidative carbonylation of methanol on Cu-exchanged Y, ZSM-5, and Mordenite

Yihua Zhang, Daniel N. Briggs, Emiel de Smit, Alexis T. Bell *

Department of Chemical Engineering, University of California, Berkeley, CA 94720-1462, USA

Received 22 May 2007; revised 15 July 2007; accepted 17 July 2007

Available online 4 September 2007

Abstract

The aim of this work was to establish the effects of zeolite structure/chemical composition on the activity and selectivity of Cu-exchanged Y (Si/Al = 2.5), ZSM-5 (Si/Al = 12), and Mordenite (Si/Al = 10) for the oxidative carbonylation of methanol to DMC. Catalysts were prepared by solid-state ion-exchange of the H-form of each zeolite with CuCl and were then characterized by FTIR and X-ray absorption spectroscopy (XAS). The XANES portion of the XAS data showed that all of the copper was present as Cu^+ cations, and analysis of the EXAFS portion of the data shows the Cu^+ cations had a Cu–O coordination number of ∼2.1 on Cu-Y and ∼2.7 on Cu-ZSM-5 and Cu-MOR. Dimethyl carbonate (DMC) was observed as the primary product when a mixture of $CH_3OH/CO/O_2$ was passed over Cu-Y, whereas dimethoxy methane was the primary product over Cu-ZSM-5 and Cu-MOR. The higher activity and selectivity of Cu-Y for the oxidative carbonylation of methanol can be attributed to the weaker adsorption of CO on the Cu^+ cations exchanged into Y zeolite. In situ IR observations revealed that under reaction conditions, adsorbed CO was displaced by methoxide groups bound to the Cu^+ cations. The kinetics of DMC synthesis suggests that the rate-limiting step in the formation of this product was the insertion of CO into Cu–OCH_3 bonds. The yield of DMC decreased with methanol conversion, likely due to the hydrolysis of DMC to methanol and carbon dioxide.

Keywords: Dimethyl carbonate; Methanol; Oxidative carbonylation; Cu-Y; Cu-ZSM-5; Cu-MOR

1. Introduction

Dimethyl carbonate (DMC) can be used as a fuel additive to replace methyl *tert*-butyl ether (MTBE), a precursor for synthesis of carbonic acid derivatives, as a methylating agent to replace methyl halides and dimethyl sulfate, and as an intermediate in the synthesis of polycarbonates and isocyanates [1–3]. Cu-exchanged zeolites have been shown to be active catalysts for the oxidative carbonylation of methanol to dimethyl carbonate, with the principal byproducts being dimethoxymethane (DMM) and methyl formate (MF) [4–9]. Previous studies have shown that the structure and chemical composition of the zeolite influence the activity and selectivity of Cu-exchanged zeolites. For example, Anderson and Root [7] have reported that Cu-X has greater activity and selectivity for DMC formation than Cu-ZSM-5. The authors proposed that CO adsorption has a negative effect on the formation of DMC. However, the mechanism by which zeolite structure and chemical composition affect the adsorptive and catalytic properties of the catalyst have not been investigated.

The present study was undertaken with aim of assessing the effects of zeolite structure on the activity and selectivity of Cu-exchanged zeolites for the synthesis of DMC. Catalysts were prepared by solid-state ion exchange of H-Y, H-ZSM-5, and H-MOR with CuCl under conditions chosen to minimize the retention of occluded CuCl [8–10]. All catalysts were characterized after preparation by infrared (IR) spectroscopy, to establish the extent to which Brönsted acid OH groups had been exchanged for copper cations, and by XANES, to establish the valence of the exchanged copper cations. The coordination of Cu to framework oxygen atoms was probed by EXAFS. The ac-

* Corresponding author. Fax: +1 510 642 4778.
E-mail address: bell@cchem.berkeley.edu (A.T. Bell).

0021-9517/$ – see front matter
doi:10.1016/j.jcat.2007.07.018

tivity and selectivity of Cu-Y, Cu-ZSM-5, and Cu-MOR were then explored for various conditions. In situ IR and XANES measurements also were carried out to identify the nature of the adsorbed species associated with the copper cations and the oxidation state of the copper cations during the oxidative carbonylation of methanol.

2. Experimental

2.1. Catalyst preparation and characterization

Cu-exchanged zeolites were prepared by solid-state ion exchange (SSIE) of the protonated form of each zeolite (Y:Si/Al = 2.5, Strem; ZSM-5:Si/Al = 12, ALSI-PENTA; MOR:Si/Al = 10, Zeolyst) with CuCl at elevated temperature in a flow of He. Details of this procedure have been described elsewhere [8–11]. Freshly prepared catalysts, designated as Cu-Y, Cu-ZSM-5, and Cu-MOR, were stored in a drybox before use. The level of proton exchange was evaluated by observing the intensity of the IR band for residual Brönsted acid sites.

The oxidation state of Cu in the Cu-exchanged zeolites was determined by Cu K-edge X-ray absorption near-edge spectroscopy (XANES). These data were acquired in transmission mode at the Stanford Synchrotron Radiation Laboratory (SSRL) on beamline 2–3. This beamline is equipped with a double-crystal monochromator, Si(111), detuned to 70% intensity to minimize the presence of higher harmonics. The samples were pressed into self-supporting wafers (calculated to have an absorbance of 2.5) and then mounted in a controlled-atmosphere cell operated at 101 kPa. Following characterization by XAS, each sample was cooled to 298 K before exposure to a particular gas or gas mixture. In separate experiments, pretreated Cu-exchanged zeolites were exposed to mixtures of He/CH_3OH, He/CO, and $He/CO/O_2/CH_3OH$. Methanol vapor was introduced using a gas saturator containing liquid methanol at 298 K. To examine the effects of gas adsorption, the sample was exposed to a flow of gas at room temperature, and the temperature was then raised at 10 K min^{-1} to 403 K and held at this level for 1 h. All XAS measurements were made in situ. Cu XANES data were analyzed using the IFEFFIT package [12,13]. Pre-edge absorptions due to the background and detector were subtracted using a linear fit to the data in the range of −200 to 50 eV relative to the sample edge energy (E_0). Each spectrum was normalized by a constant determined by the average absorption in the range of 100–300 eV relative to E_0. The edge energy of each sample and reference was taken at the first inflection point beyond any pre-edge peaks.

Extraction of the EXAFS data from the measured absorption spectra was performed with the XDAP code [14]. The pre-edge was subtracted using a modified Victoreen curve. The background was subtracted using cubic spline routines with a continuously adjustable smooth parameter. Normalization was performed by dividing the data by the height of the absorption edge at 50 eV.

Data analysis was performed by multiple-shell fitting in R-space using the EXAFS data analysis program XDAP, which allows minimization of the residuals between both the magnitude and the imaginary part of the Fourier transforms of the data and the fit. R-space fitting has significant advantages over the usually applied fitting in k-space, as has been explored in depth by Koningsberger et al. [15]. Theoretical phase shift and backscattering amplitude for the Cu–O absorber-scatterer pair, generated using the FEFF8 code, were used in EXAFS data analysis. The theoretical references were calibrated using experimental data for Cu_2O as described previously [10,16].

2.2. Measurement of catalyst activity and selectivity

Measurements of catalyst activity and selectivity were carried out using 150 mg of catalyst loaded into a 10-mm-i.d. quartz tubular flow reactor. Before being exposed to reactants, the catalyst was pretreated at 873 K for 1 h in a stream of high-purity He (99.999%). For the catalytic experiment, a CO/O_2 mixture (25.0% CO, 2.5% O_2, balance He) and He (99.999%) were used. Methanol (CH_3OH) was introduced by passing the CO/O_2 mixture through a saturator maintained at a constant temperature of 293 K. The reaction products were analyzed by gas chromatography equipped with a capillary column (Alltech, AT aquawax; polyethylene glycol stationary phase) connected to a flame ionization detector (FID) and by a packed column (Alltech, Haysep DB packing) connected to a thermal conductivity detector (TCD). The effects of feed space velocity were investigated using a $CH_3OH/O_2/CO/He$ mixture (4.0/1.0/9.0/19.3). The flow rate of this mixture was varied from 3 to 80 cm^3/min while the catalyst temperature was maintained at 403 K. A second series of experiments designed to study the effects of CO, CH_3OH, and O_2 partial pressures on reaction rate and product selectivity was carried out using a fresh sample of Cu-exchanged zeolite. In this case, the total flow rate of feed was maintained at 20 cm^3/min, and the catalyst temperature was 403 K.

Product selectivity was determined using the following equations:

$$S_{\mathrm{DMC/CO}} = [\mathrm{DMC}]/\big([\mathrm{DMC}] + [\mathrm{CO_2}]\big)$$

and

$$S_{i/\mathrm{CH_3OH}} = n[i]/\big(2[\mathrm{DMC}] + 2[\mathrm{MF}] + 3[\mathrm{DMM}] + 2[\mathrm{DME}]\big),$$

where i is DMC, MF, DMM, and DME and n is the number of carbon atoms derived from methanol.

2.3. IR characterization of adsorbed species

IR spectra were recorded on a Nicolet Nexus 670 FTIR spectrometer equipped with an MCT-A detector. Measurements were obtained at a resolution of 4 cm^{-1}. The catalysts were pressed into 15-mg self-supporting pellets and placed into an IR cell equipped with CaF_2 windows. Before absorbate exposure, the catalyst was heated in He at 673 K.

3. Results

3.1. Catalyst characterization

Fig. 1 illustrates the IR spectrum for the O–H stretching region. Spectra are shown for zeolites before and after SSIE. Two bands were located at 3640 and 3540 cm^{-1} for H-Y, attributable to the Brönsted acid O–H stretching vibrations located in the supercage and sodalite cage, respectively [8,17,18]. The small band at 3750 cm^{-1} was due to the silanol groups in zeolite Y. The IR spectrum of H-ZSM-5 exhibited only a single band at 3600 cm^{-1} characteristic of the Brönsted acid OH groups, along with a small silanol band at 3740 cm^{-1} [19]. The IR spectrum of H-MOR was very similar to that of H-ZSM-5, exhibiting bands at 3600 and 3740 cm^{-1} for Brönsted acid OH and silanol groups, respectively [20]. As shown in Fig. 1, bridging hydroxyl stretches disappeared after H-Y, H-ZSM-5, and H-MOR were exchanged with CuCl, suggesting that the Brönsted acid sites were replaced quantitatively by Cu^+ cations.

Cu K-edge XANES was used to determine the oxidation state of copper cations exchanged into each zeolite. Fig. 2 displays the XANES spectra of Cu-Y, Cu-ZSM-5, and Cu-MOR along with their corresponding first derivative curves. A single, well-defined pre-edge peak at 8983.8 eV can be seen on all three catalysts. This feature has been assigned to the degenerate $1s–4p_{x,y}$ electron transition of Cu^+ cations, which are doubly or triply coordinated in a linear or planar configuration, respectively [10,21,22]. The absence of Cu^{2+} and Cu^0 features rules out the presence of CuO or Cu metal species in copper-exchanged samples. The absence of a peak at 8987.3 eV in the XANES region also suggests the absence of any bulk CuCl. The greater intensity of the pre-edge feature for Cu-Y compared with Cu-ZSM-5 or Cu-MOR implies that Cu^+ sites in Cu-Y have a more unsaturated coordination to the zeolite framework.

The local environment of Cu^+ cations in Cu-exchanged zeolites was further analyzed using Cu K-edge EXAFS. The Fourier transforms of the k-weighted scattering function, $\chi(k)$, for Cu-exchanged zeolites are shown in Fig. 3. The main contributions can be seen to lie in the range of 1.0–2.0 Å due

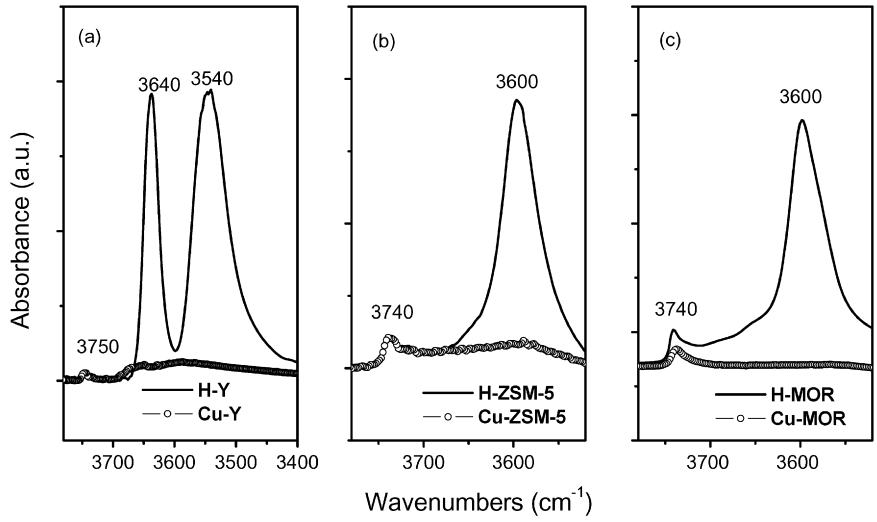

Fig. 1. IR spectra of catalysts before and after exchange of the zeolite with CuCl: (a) H-Y, Cu-Y; (b) H-ZSM-5, Cu-ZSM-5; (c) H-MOR, Cu-MOR.

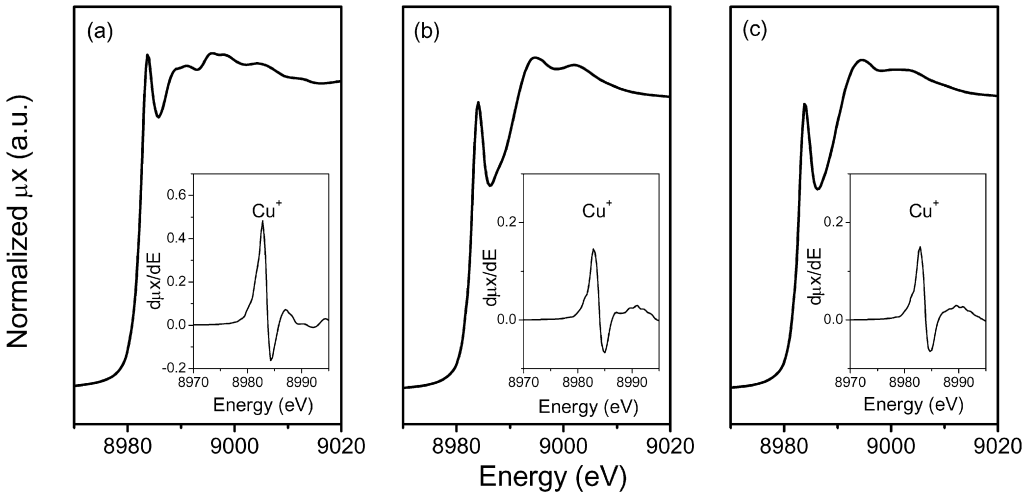

Fig. 2. Cu K-edge XANES of (a) Cu-Y; (b) Cu-ZSM-5; (c) Cu-MOR.

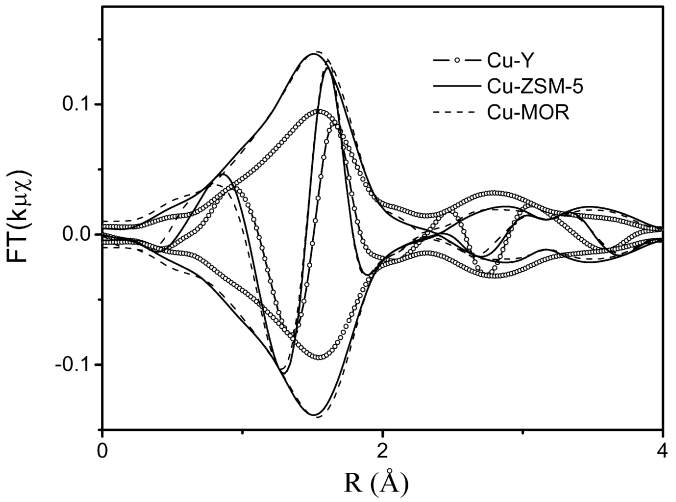

Fig. 3. Fourier transforms of experimental data for Cu-exchanged zeolites (k^1 weighted, $\Delta k = 3$–13 Å^{-1}, phase-uncorrected).

Table 1
Fit parameters of EXAFS spectra (Δk: 3–13 Å^{-1}, ΔR: 1.0–2.0 Å) and variances for model spectra of Cu-Y, Cu-ZSM-5 and Cu-MOR

Catalyst	Scatterer	N (±10%)	R (Å, ±0.02 Å)	$\Delta\sigma^2$ (10^{-3} Å^2, ±5%)	ΔE_0 (eV, ±10%)
Cu-Y	O	2.1	1.99	3.7	1.1
Cu-ZSM-5	O	2.7	1.96	3.3	−1.5
Cu-MOR	O	2.7	1.96	3.3	−1.9

to backscattering from framework oxygen atoms. The EXAFS patterns for Cu-ZSM-5 and Cu-MOR were nearly identical and differed from that for Cu-Y. Analysis of the EXAFS data for copper-exchanged zeolite catalysts was performed by multiple shell fitting in R space over the range of $1 < R < 2$ Å. Cl backscattering was not included for the fitting, for which the contribution has been proven negligible [10]. The EXAFS coordination parameters are given in Table 1. For Cu-Y, the Cu–O first shell coordination number was 2.1, and the Cu–O bond distance was 1.99 ± 0.02 Å, compared with respective values of 2.7 and 1.96 ± 0.02 Å for Cu-ZSM-5 and Cu-MOR. These observations agree with the XANES findings showing a more intense pre-edge feature on Cu-Y than on Cu-ZSM-5 or Cu-MOR, implying more unsaturated local coordination for Cu^+ sites in Cu-Y.

3.2. CO-TPD

Fig. 4 compares CO-TPD spectra for Cu-Y, Cu-ZSM-5, and Cu-MOR. The TPD spectra for Cu-ZSM-5 and Cu-MOR were very similar, exhibiting a well-resolved peak at ∼370 K followed by a very broad tail to 720 K on Cu-ZSM-5 and to 680 K on Cu-MOR. The total amount of CO adsorbed per Cu^+ cation was 0.82 for Cu-ZSM-5 and 0.70 for Cu-MOR. The TPD spectrum for Cu-Y was quite different from that for Cu-ZSM-5 and Cu-MOR, exhibiting two peaks at 388 and 425 K and complete CO desorption at 560 K. In this case, the amount of CO adsorbed per Cu^+ cation was 0.51.

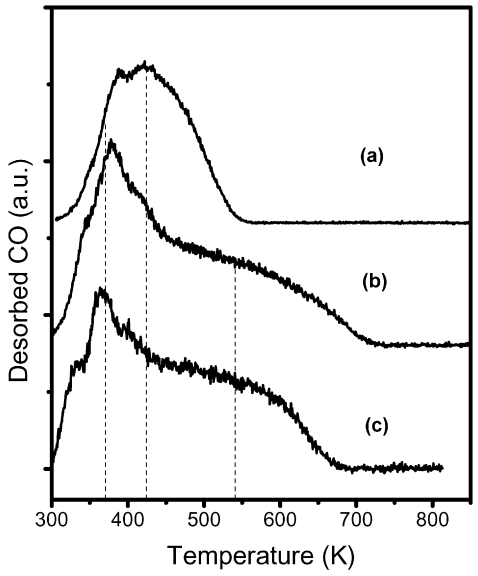

Fig. 4. CO temperature-programmed desorption spectra for Cu-Y (a), Cu-ZSM-5 (b), and Cu-MOR (c).

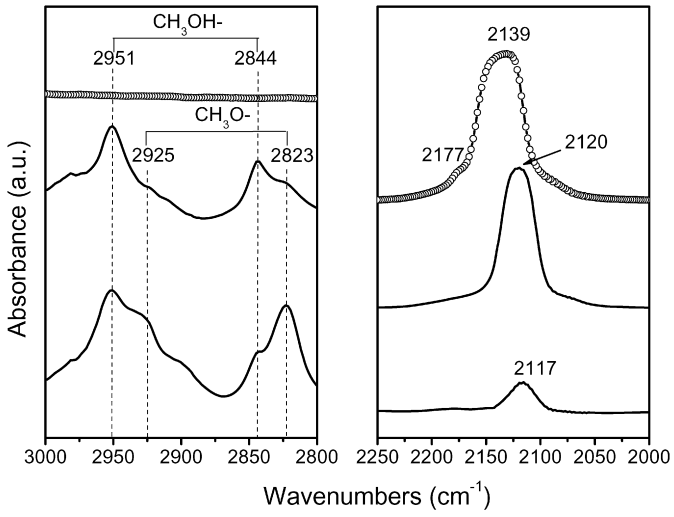

Fig. 5. IR spectra of Cu-Y in the presence of different gases (from top to bottom, CO; CO/CH_3OH; $CO/CH_3OH/O_2$).

3.3. Adsorbed species on Cu-exchanged zeolites

The nature of adsorbed species present on the Cu-exchanged zeolites was investigated by IR spectroscopy. IR spectra for Cu-Y, Cu-ZSM-5, and Cu-MOR are presented in Figs. 5, 6, and 7 for three scenarios: in the presence of CO, CO plus methanol, and CO plus methanol and oxygen. As shown in Fig. 5 for Cu-Y, when CO (20.2 kPa) was the only adsorbate, carbonyls were formed on Cu^+ cations, which exhibited a broad stretching band at 2139 cm^{-1} [8]. After addition of CH_3OH (12.12 kPa), features for molecularly adsorbed methanol appeared at 2951 and 2844 cm^{-1}, attributable to antisymmetric and symmetric C–H stretching vibrations, respectively [4,8]. At the same time, a red shift from 2139 to 2120 cm^{-1} appeared in the C–O stretching vibration. This pattern can be attributed to the co-adsorption of methanol on the Cu^+ cation to which CO is

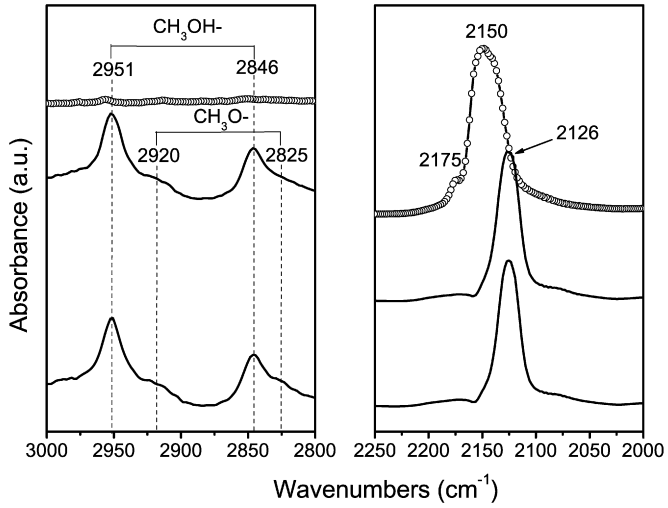

Fig. 6. IR spectra of Cu-ZSM-5 in the presence of different gases (from top to bottom, CO; CO/CH_3OH; $CO/CH_3OH/O_2$).

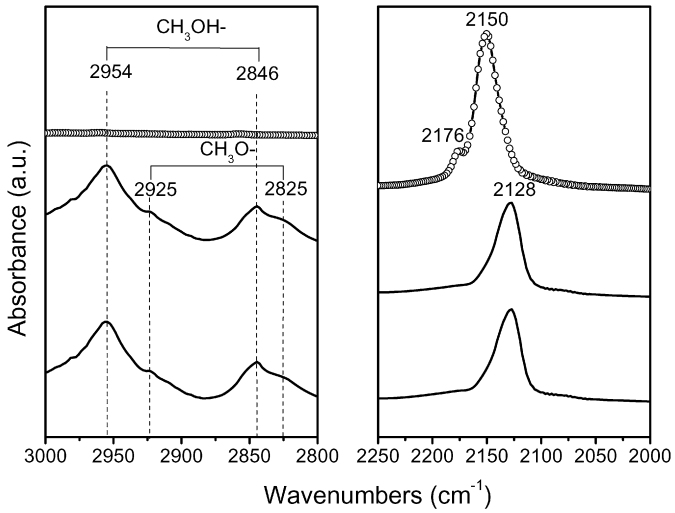

Fig. 7. IR spectra of Cu-MOR in the presence of different gases (from top to bottom, CO; CO/CH_3OH; $CO/CH_3OH/O_2$).

adsorbed. As a consequence of electron donation from adsorbed methanol, the electron density on the Cu^+ cations increased and resulted in a greater degree of back-donation of electron density from the d-orbitals of Cu to the antibonding orbital of CO. The net effect of the electron flow was to decrease the force constant of the C–O bond, which in turn caused a red shift in the C–O stretching frequency. When O_2 was introduced into the system, two new bands appeared at 2925 and 2823 cm^{-1}, assigned to symmetric and antisymmetric vibrations of C–H bonds in methoxide species [4,8]. When both methanol and oxygen were present, the CO band remained at the frequency seen in the presence of CO plus methanol, but the band intensity was ∼10% of that observed when CO alone was present. This observation indicates that once formed, methoxide species displaced the adsorption of CO. Recent quantum mechanical calculations support this conclusion [23].

Fig. 6 shows IR spectra for a series of experiments using Cu-ZSM-5, which are similar to those shown in Fig. 5 for Cu-Y. The carbonyl species on Cu-ZSM-5 was located at 2150 cm^{-1} [9]. When methanol and CO were present together, the position of the CO band red shifted to 2126 cm^{-1}. However, in contrast to what was observed for Cu-Y, the addition of oxygen to the gas stream present over the catalyst did not alter the spectrum any further, and very little evidence for the formation of methoxide species could be observed in the C–H stretching region of the spectrum. This clearly indicates that the concentration of surface methoxide species was much lower on Cu-ZSM-5 than on Cu-Y. Fig. 7 shows that the behavior of Cu-MOR was similar to that of Cu-ZSM-5 and, again, different from that of Cu-Y.

3.4. Cu XANES for Cu-exchanged zeolites in DMC synthesis

The oxidation state and coordination of Cu were probed by Cu K-edge XANES under reaction conditions. Because changes in the XANES features were observed more clearly in the derivative mode, only such data are presented here. As shown in Figs 8a, 8d, and 8g, when the catalysts were exposed to CH_3OH at 403 K, the pre-edge peak of Cu^+ remained at the position observed under He but slightly decreased in intensity. This suggests that the molecular adsorption of CH_3OH on Cu^+ sites did not affect the oxidation state of Cu and influenced its coordination only slightly. When He-treated Cu-exchanged zeolites were exposed to 20.2 kPa of CO at 403 K, the resonant peak at ∼8983 eV associated with coordinatively unsaturated Cu^+ observed in He and/or methanol treated samples was replaced by a new feature at ∼8981 eV (Figs. 8b, 8e, and 8h). These changes in the near-edge region are due to the changes in the coordination of Cu^+ cations resulting by the formation of carbonyl complexes [22,24]. Thus, the formation of the new feature can be considered a characteristic of CO adsorption. When Cu-Y was exposed to a $CH_3OH/CO/O_2$ mixture (12.12/20.2/2.02 kPa) at 403 K, the first derivative spectrum (Fig. 8c) shows that the peak at ∼8983 eV was restored to a level very similar to that observed when the catalyst was under He or CH_3OH. The peak at ∼8981 eV due to CO adsorption became negligible. The XANES data together with the IR spectra shown in Fig. 5 suggest that on exposure of Cu-Y containing preadsorbed CO to a $CH_3OH/CO/O_2$ mixture (DMC synthesis conditions), CO was displaced significantly by adsorbed methanol and methoxide species. A different pattern can be seen on Cu-ZSM-5 and Cu-MOR for similar conditions. The first derivative spectrum (Figs. 8f and 8i) shows two well-defined peaks at ∼8981 and ∼8983 eV. The positions of these two features were identical to those observed under CO or CH_3OH, respectively. In agreement with the IR spectra shown in Figs. 6 and 7, the XANES data recorded on exposure of Cu-ZSM-5 or Cu-MOR to a $CH_3OH/CO/O_2$ mixture showed no significant evidence for the displacement of CO by methanol and methoxide species, as was seen for Cu-Y. Thus, for Cu-ZSM-5 and Cu-MOR, the principal species observed under reaction conditions were CO and CH_3OH co-adsorbed on Cu^+ cations.

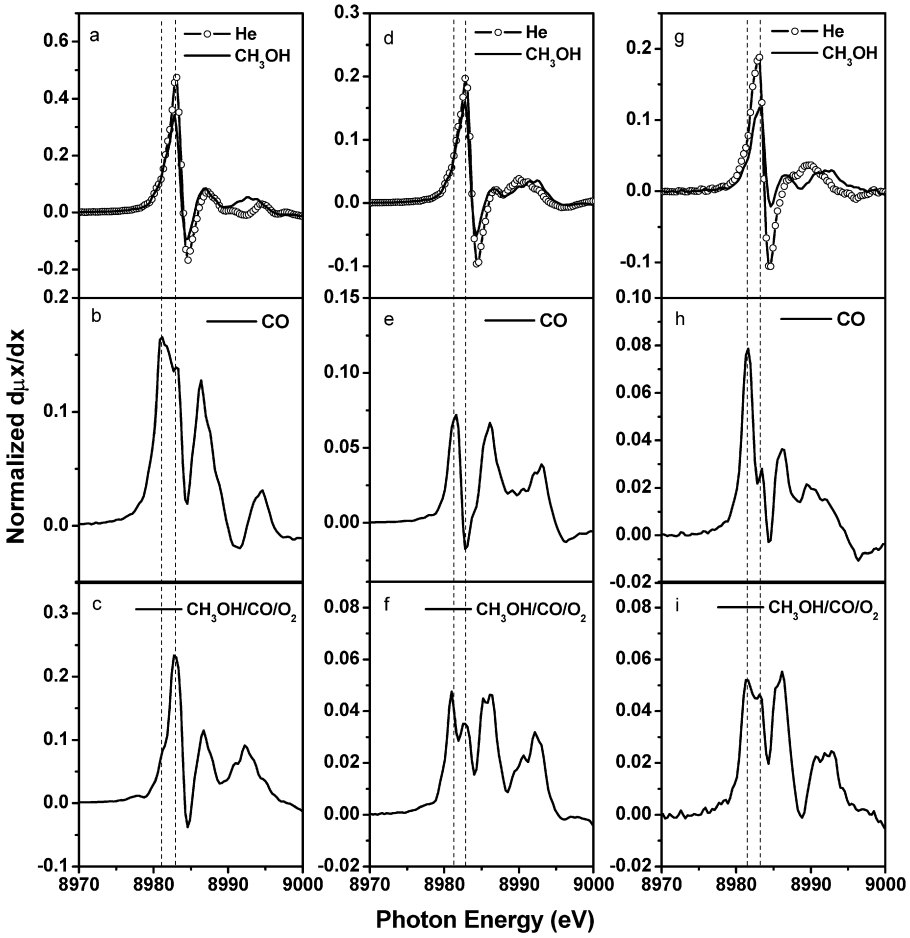

Fig. 8. The first derivative curves of Cu K-edge XANES on Cu-Y (a–c); Cu-ZSM-5 (d–f); Cu-MOR (g–i) under different atmosphere.

3.5. Catalytic activity and selectivity

Fig. 9 displays the effects of methanol conversion on the rates of product formation and the corresponding product selectivities for Cu-Y, Cu-ZSM-5, and Cu-MOR. All experiments were carried out at 403 K and 101 kPa with a feed containing $CH_3OH/CO/O_2$ in the ratio 12.12/20.2/2.02 kPa. In each case, 150 mg of catalyst was used, and the methanol conversion was varied by changing the flow rate of the feed mixture. The carbon-containing products observed included DMC, DMM, MF, DME, and CO_2. The overall activity at a given methanol conversion was greatest for Cu-Y and declined in the order Cu-Y > Cu-ZSM-5 ≫ Cu-MOR. The distribution of products also was a strong function of zeolite structure. For an extrapolated conversion of zero, the selectivity to DMC was about 84% for Cu-Y, 50% for Cu-ZSM-5, and only 35% for Cu-MOR. However, with increasing methanol conversion, the selectivity to DMC for all catalysts decreased, paralleled by an increased rate of CO_2 formation.

DMM was the second most prevalent product formed from methanol. At zero conversion, the selectivity to DMM from methanol was 10% for Cu-Y, 40% for Cu-ZSM-5, and 35% for Cu-MOR. The selectivity to this product rose with increasing methanol conversion. Small amounts of MF and DME were formed on all three catalysts. For an extrapolated conversion of zero, the selectivity to MF was highest on Cu-MOR (25%) and lowest on Cu-Y (5%). Only small changes in the selectivity to MF were observed for any of the catalysts with increasing methanol conversion. DME was formed to a very limited extent on Cu-Y; however, modest selectivity to this product was seen for Cu-ZSM-5 and Cu-MOR. The selectivity to DME increased with methanol conversion for both Cu-Y and Cu-ZSM-5 but remained almost constant for Cu-MOR.

The influence of reactant partial pressures is illustrated in Figs. 10–12. All of these data were obtained at 403 K, a total pressure of 101 kPa, and a fixed space-time. An increase in CO partial pressure caused a strong increase in the rate of DMC and CO_2 formation on Cu-Y but had little effect on the formation of DMM, MF, or DME. A similar pattern with respect to DMC and CO_2 formation was found for Cu-MOR, but in this case, the rate of DMM formation was relatively insensitive to CO partial pressure, whereas the rates of MF and DME formation declined with increasing CO partial pressure. For Cu-ZSM-5, the rates of DMC and CO_2 formation showed a more modest increase with increasing CO partial pressure than was seen for Cu-Y or Cu-MOR. However, in contrast to the other catalysts, the rates of DMM, MF, and DME formation decreased with increasing CO partial pressure.

The rate of DMC formation for Cu-Y and Cu-ZSM-5 passed through a broad maximum with increasing methanol partial

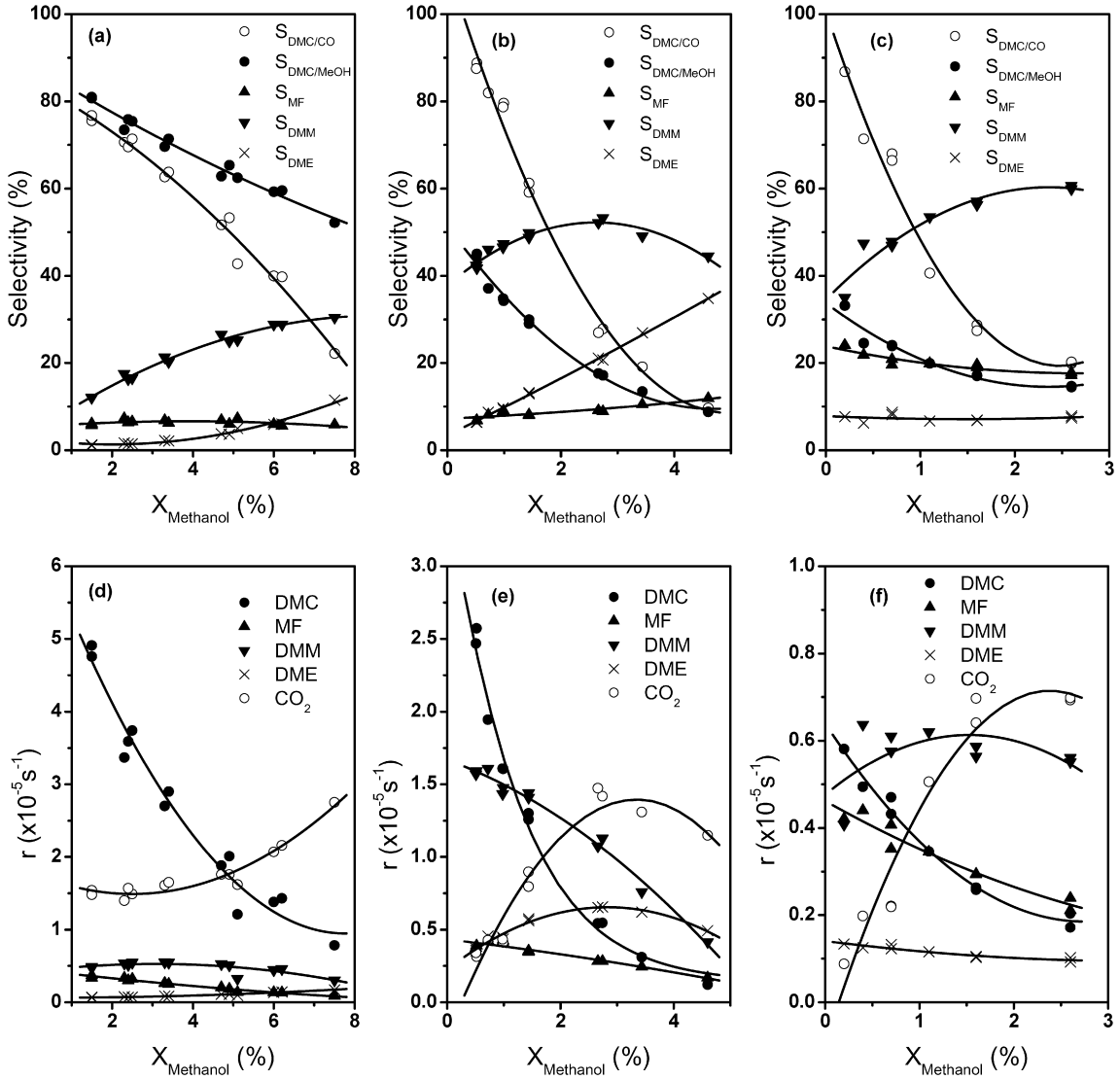

Fig. 9. Selectivities and production rates as a function of methanol conversion (achieved by varying the feed residence time) on Cu-Y (a, d), Cu-ZSM-5 (b, e), Cu-MOR (c, f) at 403 K under $CH_3OH/CO/O_2$ (12.12/20.2/2.02 kPa).

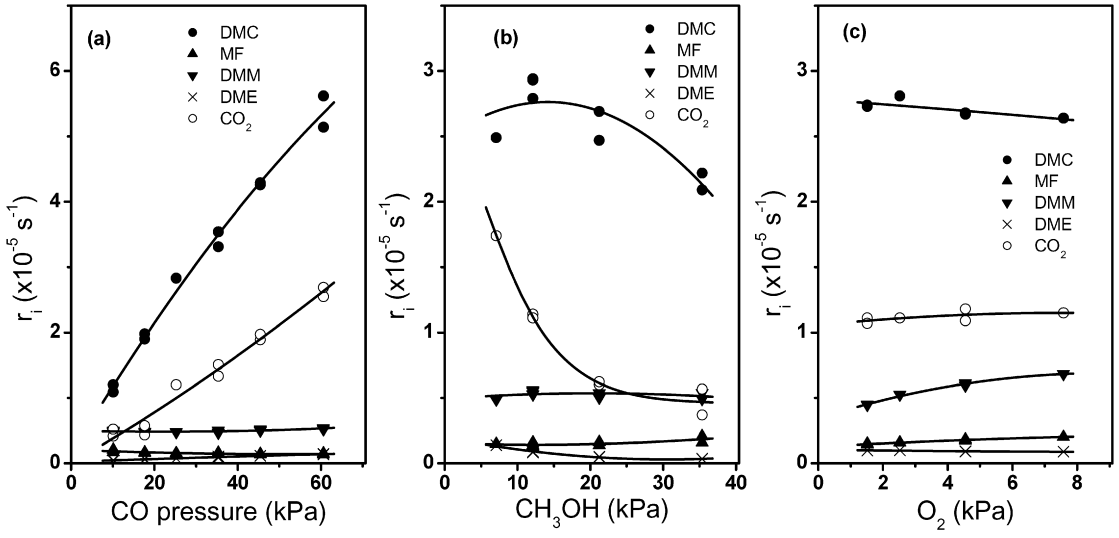

Fig. 10. Effect of reactant partial pressure on oxidative carbonylation of methanol at 403 K on Cu-Y: (a) CO (CH_3OH 12.12 kPa; O_2 2.53 kPa); (b) CH_3OH (CO 25.25 kPa, O_2 2.53 kPa); (c) O_2 (CO 25.25 kPa, CH_3OH 12.12 kPa).

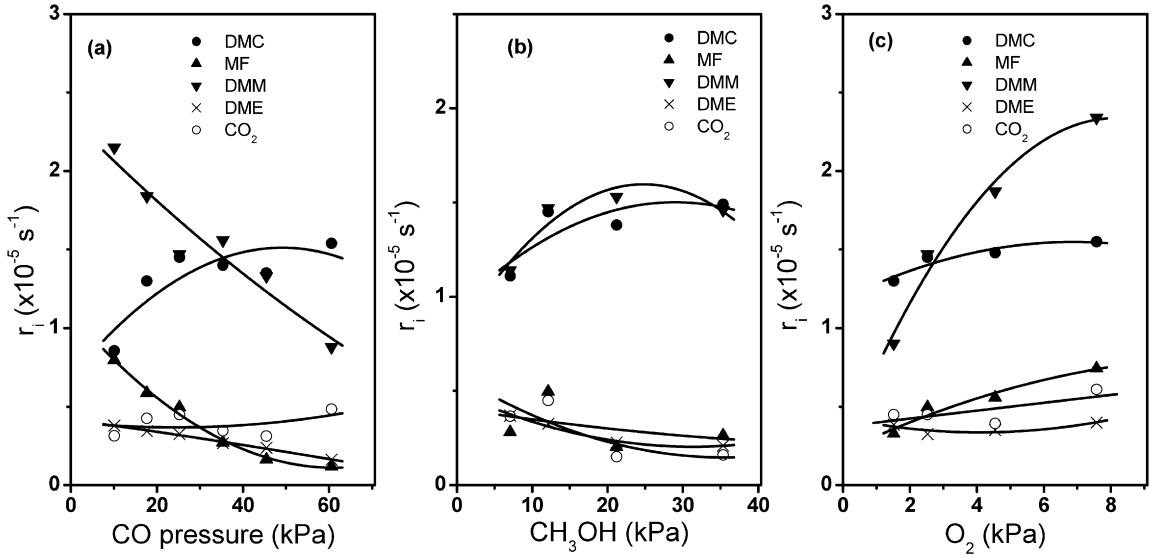

Fig. 11. Effect of reactant partial pressure on oxidative carbonylation of methanol at 403 K on Cu-ZSM-5: (a) CO (CH_3OH 12.12 kPa; O_2 2.53 kPa); (b) CH_3OH (CO 25.25 kPa, O_2 2.53 kPa); (c) O_2 (CO 25.25 kPa, CH_3OH 12.12 kPa).

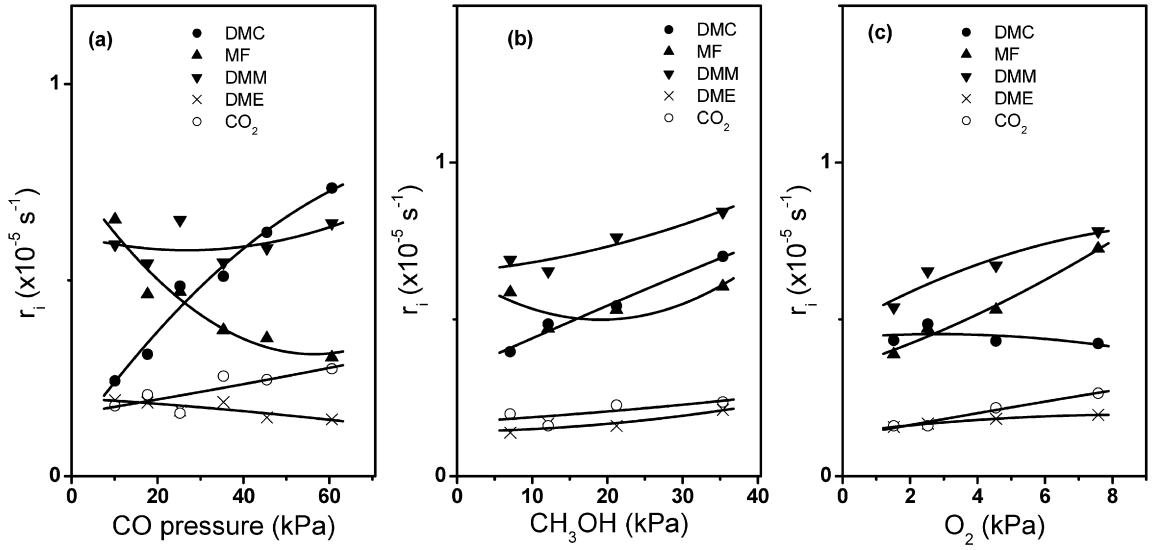

Fig. 12. Effect of reactant partial pressure on oxidative carbonylation of methanol at 403 K on Cu-MOR: (a) CO (CH_3OH 12.12 kPa; O_2 2.53 kPa); (b) CH_3OH (CO 25.25 kPa, O_2 2.53 kPa); (c) O_2 (CO 25.25 kPa, CH_3OH 12.12 kPa).

pressure, whereas for Cu-MOR, the rate of DMC formation increased monotonically with increasing methanol partial pressure. For Cu-Y, the rates of DMM and MF formation showed negligible changes with increasing methanol partial pressure, whereas the rates of CO_2 and DME formation decreased with increasing methanol partial pressure. The dependence of the rate of DMM formation on Cu-ZSM-5 was similar to that observed for DMC, whereas the rates of all other products decreased with increasing methanol partial pressure. In contrast, for Cu-MOR, the rate of MF formation passed through a shallow minimum, but the rates of DMM, DME, and CO_2 formation increased with increasing methanol partial pressure.

The effects of O_2 partial pressure on the rates of product formation were more similar for all three catalysts than those observed for changes in the CO and methanol partial pressures. The rate of DMC formation decreased slightly with increasing O_2 partial pressure for Cu-Y and Cu-MOR but increased for Cu-ZSM-5. However, the rates of DMM, MF, and CO_2 formation increased with increasing O_2 partial pressure for all three catalysts.

4. Discussion

4.1. Catalyst characterization

Complete exchange of Brönsted acid protons in H-Y, H-ZSM-5, and H-MOR by copper cations was achieved by SSIE, as evidenced by disappearance of the IR band for Brönsted acid hydroxyl groups. Cu K-edge XANES demonstrated that independent of the zeolite framework structure and Si/Al ra-

tio, all of the exchanged copper was present as Cu^+ in the as-prepared catalyst. Differences in the Cu–O coordination and bond lengths were demonstrated by Cu K-edge EXAFS. The Cu–O coordination number decreased in the order $N_{Cu\text{-}ZSM\text{-}5} = N_{Cu\text{-}MOR} > N_{Cu\text{-}Y}$, whereas the average Cu–O bond distance increased in the order $R_{Cu\text{-}ZSM\text{-}5} = R_{Cu\text{-}MOR} < N_{Cu\text{-}Y}$.

The IR spectroscopy of adsorbed CO provided limited evidence for difference in the properties of Cu^+ cations exchanged into zeolites Y, ZSM-5, and MOR. As shown in Figs. 5–7, the IR spectrum of adsorbed CO consisted of two or more overlapping bands in the region of 2139–2150 cm^{-1}. The band for CO adsorbed on Cu-Y was broader than that for CO adsorbed on either Cu-ZSM-5 or Cu-MOR, particularly on the low-frequency side, and the bands for CO adsorbed on Cu-ZSM-5 and Cu-MOR were of very similar shape and position. DFT calculations for CO adsorbed on Cu-ZSM-5 and Cu-Y showed that the vibrational frequencies for the two zeolites were very similar and that there was no obvious correlation of band position with the zeolite framework structure or Si/Al ratio [25].

The most significant effect of zeolite structure and Si/Al ratio on the properties of Cu^+-exchanged Y, ZSM-5, and MOR were revealed by the CO TPD spectra presented in Fig. 4. This clearly shows that complete desorption of CO occurred at a significantly lower temperature for Cu-Y than for Cu-ZSM-5 and Cu-MOR, which exhibited very similar TPD spectra. The total amount of CO adsorbed at 298 K per Cu^+ cation also reflects the zeolite structure and the Si/Al ratio; CO/Cu was 0.51 for Cu-Y, compared with 0.82 for Cu-ZSM-5 and 0.70 for Cu-MOR. These results are consistent with experimentally measured heats of CO adsorption. Calorimetric measurements of the heat of CO adsorption on Cu-Y are reported to be in the range of 15.5–19.1 kcal/mol [26], whereas values of 23.8–31 kcal/mol have been reported for Cu-ZSM-5 [27,28]. DFT calculations have shown that the heat of CO adsorption in Cu-Y is 15.0 kcal/mol, compared with 24–33 kcal/mol for Cu-ZSM-5 [25]. These calculations also have shown that the strength of CO adsorption is more sensitive to the Si/Al ratio than to the local structure of the exchange site, which reflects the framework structure of the zeolite. Thus, the lower heat of CO adsorption for Cu-Y is a direct consequence of its lower Si/Al ratio (2.5) compared with that of Cu-ZSM-5 (12) and Cu-MOR (10).

4.2. Catalyst activity and selectivity

The results presented in Figs. 9 and 10 demonstrate clearly that Cu-Y is a more active catalyst for DMC synthesis than either Cu-ZSM-5 or Cu-MOR. The rate of DMC synthesis increased significantly with increasing CO partial pressure, was independent of O_2 partial pressure, and passed through a broad maximum with CH_3OH partial pressure. Some DMM was produced over Cu-Y, but at low methanol conversion, selectivity to this product was only 10%. The only other product seen in significant concentration was CO_2. The formation of CO_2 also increased strongly with CO partial pressure, was insensitive to O_2 partial pressure, and decreased with increasing CH_3OH partial pressure. As the conversion of methanol increased, the rate of DMC synthesis declined, whereas the rate of CO_2 formation increased. This trend is likely due to the reaction of DMC and H_2O, both of which are formed under reaction conditions, to produce methanol and CO_2 via reaction (1) [1].

$$H_2O + (CH_3O)_2CO \rightarrow 2CH_3OH + CO_2. \quad (1)$$

Because the ΔG^0 for this reaction is −12.2 kcal/mol, it should occur spontaneously.

Insights into the processes involved in the formation of DMC can be gained from the in situ IR and XANES spectra given in Figs. 5 and 8, respectively. Fig. 5 shows that under DMC synthesis conditions, the amount of adsorbed CO decreased considerably relative to what was observed in the presence of CO alone and that the position of the CO band was red-shifted by 22 cm^{-1}. Features of adsorbed methanol and methoxide species also can be clearly seen under the reaction conditions. The derivative XANES patterns shown in Fig. 8 confirm that under DMC synthesis conditions, the fraction of the Cu^+ cations interacting with CO diminished significantly relative to that observed in the presence of CO alone. These observations suggest that under reaction conditions, methoxide species were formed at the Cu^+ sites, and that the formation of these species inhibited the adsorption of CO. Quantum calculations indicate that CO could adsorb weakly on a Cu^+ cation containing a single methoxide species, but not on one containing a methoxide species and a second ligand, such as OH, OOH, or OCH_3 [23]. It also is noted that when the formation of methoxide species is limited (as is the case on Cu-ZSM-5 and Cu-MOR), the rate of DMC formation is reduced significantly (see Figs. 9e and 9f). Therefore, the formation of methoxide species appears to be an essential first step on the pathway to DMC formation. As shown below, DMC may form via one of two pathways. The first is by the addition of gas-phase or weakly adsorbed CO to a species such as $Z^-[Cu^+(OH)(OCH_3)]$ to produce $Z^-[Cu^+(OH)(O(CO)CH_3)]$ [reaction (3)]. The addition of CH_3OH to the latter species would produce DMC and H_2O [reaction (4)]. This pathway is similar to that proposed by King [4,5] and by Anderson and Root [6,7]. Alternatively, CH_3OH may be first added to $Z^-[Cu^+(OH)(OCH_3)]$ to produce $Z^-[Cu^+(OCH_3)_2]$ plus water via reaction (5), after which CO reacts with the dimethoxide to form DMC [reaction (6)]. The latter route appears to be preferred, because exposure of Cu-Y containing methoxide species prepared by exposure of the catalyst to a mixture of CH_3OH and O_2 at 403 K to CO in He resulted in the immediate appearance of DMC in the gas phase and the observation by IR spectroscopy of bands attributable to DMC adsorbed on Cu-Y. These reactions are as follows:

$$Z[CuO] + CH_3OH \rightarrow Z[Cu(OH)(OCH_3)], \quad (2)$$

$$Z[Cu(OH)(OCH_3)] + CO \rightarrow Z[Cu(OH)(O(CO)CH_3)], \quad (3)$$

$$Z[Cu(OH)(O(CO)CH_3)] + CH_3OH \rightarrow ZCu + (CH_3O)_2CO + H_2O, \quad (4)$$

$$Z[Cu(OH)(OCH_3)] + CH_3OH \rightarrow Z[Cu(OCH_3)_2] + H_2O, \quad (5)$$

$$Z[Cu(OCH_3)_2] + CO \rightarrow ZCu + (CH_3O)_2CO. \quad (6)$$

Compared with Cu-Y, Cu-ZSM-5 and Cu-MOR exhibited significantly lower activity for DMC synthesis. The rates of DMC

formation on the latter two catalysts increased with increasing CO partial pressure, in a manner similar to that observed for Cu-Y. Likewise, the rate of DMC formation was not very sensitive to the partial pressure of O_2. Increasing the partial pressure of O_2 led to an increase in the rate of DMM formation on Cu-ZSM-5 and Cu-MOR.

As noted earlier, both IR spectroscopy and XANES spectra obtained in situ demonstrate that the concentration of surface methoxide species was much lower on Cu-ZSM-5 and Cu-MOR than on Cu-Y and that most of the Cu^+ cations were occupied by adsorbed methanol and CO. The strongly adsorbed CO appeared to inhibit the formation of methoxide species and thus the formation of DMC. Therefore, reactions (4) and (6) appeared to be strongly suppressed on Cu-ZSM-5 and Cu-MOR.

DMM was formed on all three catalysts. The rates of formation of this product were comparable on Cu-Y and Cu-MOR and notably higher on Cu-ZSM-5. The participation of O_2 in the formation of this product was essential, because the overall stoichiometry of DMM formation was $3CH_3OH + (1/2)O_2 \rightarrow (CH_3O)_2CH_2 + 2H_2O$. Consistent with this, as shown in Figs. 10–12, the rate of DMM formation increased with increasing partial pressures of both CH_3OH and O_2. Because the rate of DMM formation did not appear to correlate with the formation of methoxide species, DMM may have formed via a concerted reaction involving CH_3OH and O_2; however, the results of the present study are insufficient to provide a basis for suggesting what this mechanism might be.

5. Conclusion

Our findings indicate that Cu in Cu-Y, Cu-ZSM-5, and Cu-MOR prepared by solid-state exchange of H-Y, H-ZSM-5, and H-MOR with CuCl is present exclusively as Cu^+. The average coordination number of the Cu^+ is close to 2 for Cu-Y and between 2 and 3 for Cu-ZSM-5 and Cu-MOR. Under identical reaction conditions, the activity and selectivity of these catalysts for the oxidative carbonylation of methanol is a function of the zeolite structure and Si/Al ratio. Cu-Y exhibits the greatest activity and selectivity. Cu-ZSM-5 and Cu-MOR exhibit significantly lower DMC synthesis activity and higher selectivity for DMM synthesis than Cu-Y. The superior activity and selectivity of Cu-Y for DMC synthesis are associated with its weaker adsorption of CO. Under reaction conditions, CO adsorbed on Cu-Y is gradually displaced by methoxide species attached to the Cu^+ cations. This process also occurs on Cu-ZSM-5 and Cu-MOR but to a much lesser extent. The ability of methoxide groups to displace adsorbed CO from the Cu^+ cations of Cu-Y is closely related to the weaker binding of CO. Theoretical calculations suggest that the lower binding energy of CO to Cu^+ cations in Cu-Y compared with that in Cu-ZSM-5 or Cu-MOR is due to the lower Si/Al ratio of Cu-Y. The rate of DMC synthesis was found to increase strongly with CO partial pressure and weakly with O_2 partial pressure, and to be virtually independent of CH_3OH partial pressure. These trends, in combination with in situ IR observations, suggest that the rate-limiting step for the formation of DMC is likely to be the insertion of CO into a $Cu–OCH_3$ bond. The observed loss in DMC yield with increasing methanol conversion is attributed to the hydrolysis of DMC to methanol and carbon dioxide, a thermodynamically favorable reaction.

Acknowledgments

The authors thank the synchrotron laboratories of SSRL and ALS for the allocated beam time and assistance. This work was supported by the Methane Conversion Cooperative (MC^2) funded by BP.

References

[1] M.A. Pacheco, C.L. Marshall, Energy Fuels 11 (1997) 2–29.
[2] Y. Ono, Pure Appl. Chem. 68 (1996) 367–375.
[3] Y. Ono, Appl. Catal. A Gen. 155 (1997) 133–166.
[4] S.T. King, J. Catal. 161 (1996) 530–538.
[5] S.T. King, Catal. Today 33 (1997) 173–182.
[6] S.A. Anderson, T.W. Root, J. Catal. 217 (2003) 396–405.
[7] S.A. Anderson, T.W. Root, J. Mol. Catal. A Chem. 220 (2004) 247–255.
[8] I.J. Drake, Y.H. Zhang, D. Briggs, B. Lim, T. Chau, A.T. Bell, J. Phys. Chem. B 110 (2006) 11654–11664.
[9] Y.H. Zhang, I.J. Drake, D.N. Briggs, A.T. Bell, J. Catal. 244 (2006) 219–229.
[10] Y.H. Zhang, I.J. Drake, A.T. Bell, Chem. Mater. 18 (2006) 2347–2356.
[11] I.J. Drake, Y.H. Zhang, M.K. Gilles, C.N.T. Liu, P. Nachimuthu, R.C.C. Perera, H. Wakita, A.T. Bell, J. Phys. Chem. B 110 (2006) 11665–11676.
[12] M. Newville, J. Synch. Rad. 8 (2001) 322–324.
[13] B. Ravel, M. Newville, J. Synch. Rad. 12 (2005) 537–541.
[14] M. Vaarkamp, J.C. Linders, D.C. Koningsberger, Physica B 209 (1995) 159–160.
[15] D.C. Koningsberger, B.L. Mojet, G.E. van Dorssen, D.E. Ramaker, Top. Catal. 10 (2000) 143–155.
[16] Y.H. Zhang, M.L. Toebes, A. van der Eerden, W.E. O'Grady, K.P. de Jong, D.C. Koningsberger, J. Phys. Chem. B 108 (2004) 18509–18519.
[17] U. Eichler, M. Brandle, J. Sauer, J. Phys. Chem. B 101 (1997) 10035–10050.
[18] M.W. Anderson, J. Klinowski, Zeolites 6 (1986) 455–466.
[19] A. Zecchina, S. Bordiga, G. Spoto, D. Scarano, G. Petrini, G. Leofanti, M. Padovan, C.O. Arean, J. Chem. Soc. Faraday Trans. 88 (1992) 2959–2969.
[20] C. Lamberti, S. Bordiga, A. Zecchina, M. Salvalaggio, F. Geobaldo, C.O. Arean, J. Chem. Soc. Faraday Trans. 94 (1998) 1519–1525.
[21] C. Lamberti, S. Bordiga, M. Salvalaggio, G. Spoto, A. Zecchina, F. Geobaldo, G. Vlaic, M. Bellatreccia, J. Phys. Chem. B 101 (1997) 344–360.
[22] C. Lamberti, S. Bordiga, F. Bonino, C. Prestipino, G. Berlier, L. Capello, F. D'Acapito, F.X.L.I. Xamena, A. Zecchina, Phys. Chem. Chem. Phys. 5 (2003) 4502–4509.
[23] X. Zheng, Y. Zhang, A.T. Bell, unpublished work.
[24] P. Kumashiro, Y. Kuroda, M. Nagao, J. Phys. Chem. B 103 (1999) 89–96.
[25] X. Zheng, Y. Zhang, A.T. Bell, J. Phys. Chem. C, submitted for publication.
[26] G.D. Borgard, S. Molvik, P. Balaraman, T.W. Root, J.A. Dumesic, Langmuir 11 (1995) 2065–2070.
[27] Y. Kuroda, Y. Yoshikawa, S. Emura, R. Kumashiro, M. Nagao, J. Phys. Chem. B 103 (1999) 2155–2164.
[28] A. Gervasini, C. Picciau, A. Auroux, Microporous Mesoporous Mater. 35 (6) (2000) 457–469.